Local structure and vibrational properties of α-Pu, α-U, and the α-U charge-density wave

E. J. Nelson,[1] P. G. Allen,[2] K. J. M. Blobaum,[1] M. A. Wall,[1] and C. H. Booth[3]
[1]*Materials Science and Technology Division, Lawrence Livermore National Laboratory, P.O. Box 808, Livermore, California 94551, USA*
[2]*Chemistry and Chemical Engineering Division, Lawrence Livermore National Laboratory, P.O. Box 808, Livermore, California 94551, USA*
[3]*Chemical Sciences Division, Lawrence Berkeley National Laboratory, Berkeley, California 94720, USA*
(Received 21 September 2004; published 27 May 2005)

The local atomic environment and vibrational properties of atoms in monoclinic pure α-plutonium as well as orthorhombic pure α-uranium and its low-temperature charge-density-wave (CDW) modulation are examined by extended x-ray absorption fine structure spectroscopy (EXAFS). Pu L_{III}-edge and U L_{III}-edge EXAFS data measured at low temperatures verify the crystal structures of α-U and α-Pu samples previously determined by x-ray diffraction and neutron scattering. Debye-Waller factors from temperature-dependent EXAFS measurements are fit with a correlated Debye model. The observed Pu-Pu bond correlated Debye temperature of $\theta_{cD}(\alpha\text{-Pu}) = 162 \pm 5$ K for the pure α-Pu phase agrees with our previous measurement of the correlated Debye temperature of the gallium-containing α'-Pu phase in a mixed phase 1.9 at. % Ga-doped α'-Pu/δ-Pu alloy. The temperature dependence of the U-U nearest neighbor Debye-Waller factor exhibits a sharp discontinuity in slope near $T_{CDW} = 43$ K, the transition temperature at which the charge-density wave (CDW) in α-U condenses from a soft phonon mode along the (100) direction. Our measurement of the CDW using EXAFS is the first observation of the structure of the CDW in polycrystalline α-U. The different temperature dependence of the Debye-Waller factor for $T < T_{CDW}$ can be modeled by the change in bond length distributions resulting from condensation of the charge density wave. For $T > T_{CDW}$, the observed correlated Debye temperature of $\theta_{cD}(\alpha\text{-U}) = 199 \pm 3$ K is in good agreement with other measurements of the Debye temperature for polycrystalline α-U. CDW structural models fit to the α-U EXAFS data support a squared CDW at the lowest temperatures, with a displacement amplitude of $\varepsilon = 0.05 \pm 0.02$ Å.

DOI: 10.1103/PhysRevB.71.184113 PACS number(s): 61.10.Ht, 61.66.Bi, 63.20.Dj, 71.45.Lr

I. INTRODUCTION

The actinides U and Pu are unusual metals because they adopt low-symmetry structures for their lowest-temperature crystallographic phases. The α-Pu phase is monoclinic, with eight inequivalent sites and an inversion plane in its unit cell,[1] while the α-U phase is orthorhombic with two atoms in the unit cell.[2] Söderlind *et al.* provide an explanation of the lower-symmetry crystal structures of the light actinides within a unified picture which can be applied to all metal crystal structures.[3] In this picture, the energy gain due to a crystal-structure (Peierls) distortion is compared to the opposing energy gain resulting from the electrostatic Madelung energy, which stabilizes high-symmetry structures. In the light actinides, the narrowness of the $5f$ electron bandwidth results in a greater energy gain for the crystal-structure (Peierls) distortion, and in a low-symmetry crystal structure. The α-U and α-Pu phases are the ground-state, low-temperature phases of these actinides,[4,5] and understanding the local structure and bond vibrational properties of α-U and α-Pu are important from both a fundamental condensed matter physics and applied metallurgy standpoint.

Figure 1 details the structure of the monoclinic unit cell of α-Pu, as previously determined from x-ray diffraction.[1] Within each atomic sheet perpendicular to the (010) direction, the spacing of the atoms in the unit cell is distorted from a regular pattern, resulting in a distribution of bond lengths.

The α-Pu phase exists as the stable form of Pu to temperatures above room temperature ($T_{\alpha\rightarrow\beta} = 398$ K), but alloying gallium (up to 9 at. % Ga) or other dopants with Pu stabilizes the fcc δ-Pu phase at room temperature.[6] While the $5f$ electrons are delocalized and participate in bonding in α-Pu, these electrons become localized in the δ-Pu phase, allowing rearrangement of the Pu atoms in a higher symmetry structure.[4]

Figure 2 details the structure of the orthorhombic unit cell of α-U, as previously determined from x-ray diffraction.[2]

The α-U phase has an unusual phase transition at $T_{CDW} = 43$ K, which is attributed to a charge density wave (CDW). The detailed structure of the CDW has been the object of a number of detailed neutron scattering and x-ray diffraction (XRD) experiments on single-crystal α-U.[2,7–14] The results of these experiments are compiled in a review by Lander *et al.*[15] The CDW is interpreted as the condensation of a phonon mode along the (1 0 0) direction, whose frequency drops dramatically at low temperatures (softening). This is the same direction as the straight linear chain of bonds in the undistorted structure. In the initial studies by Smith *et al.*,[8] the wave vector **q** of the CDW displacement was believed to be commensurate with the crystal lattice, and was thought to cause a doubling of the unit cell along the (100) direction, i.e., $q_x = 1/2$. Figure 2 depicts this simplified CDW structure. The U-U bonds in the (100) linear chain are modulated by a longitudinal wave, with the amplitude of the displacement wave $\boldsymbol{\varepsilon}$ predominantly along the (100) direction.

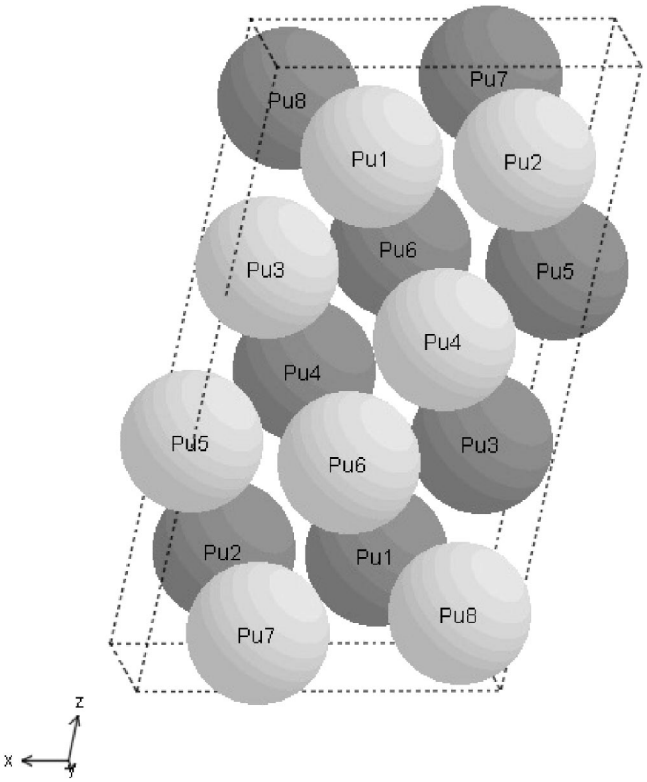

FIG. 1. Unit cell of monoclinic α-Pu. $a=6.183$ Å, $b=4.822$ Å, $c=10.963$ Å, and $\beta=101.79$ deg (from Ref. 1). There are 8 inequivalent Pu atomic sites in the unit cell (16 atoms total), and the $\langle 010 \rangle$ plane is an inversion plane.

Later studies by Marmeggi *et al.* and others[9–14] which sampled more of the reciprocal lattice space indicated a commensurate **q** in all three directions only at temperatures T below the lock-in temperature $T_{\text{lock-in}}=22$ K. For temperatures $22\ \text{K}<T<37\ \text{K}$, q_y and q_z become incommensurate, while q_x stays commensurate at $q_x=1/2$. For temperatures $37\ \text{K}<T<43\ \text{K}$, all three components of **q** are incommensurate with the crystal lattice. As for the amplitude of the displacement wave $\boldsymbol{\varepsilon}$, the predominant component still is along (100), with $\varepsilon_x=0.027\pm0.001$ Å. The resulting CDW structure looks like a frozen "optical" displacement wave along the (100) direction, with the maximum amplitude of the wave also depending on the y and z coordinates of the atoms in the CDW-expanded unit cell. In addition, diffraction experiments have detected higher-order satellites of the CDW diffraction peaks with only odd-integer indices. This suggests a "squaring" of the CDW displacement wave rather than a sine wave distribution of displacements, although a "phase slipped" sine wave model is an alternative model.[13,14] At temperatures above $T_{\text{CDW}}=43$ K, the CDW frequency becomes nonzero in time, resulting in the low-frequency phonon wave with wave vector $\mathbf{q}=(0.5,0,0)$. Manley *et al.*[16] modeled the temperature dependence of the phonon frequency softening with various vibrational potentials, and achieved the best fit with a harmonic potential. The softening is due to the force constants being temperature dependent rather than due to anharmonic potentials.

Extended x-ray absorption fine structure (EXAFS) is an excellent technique for determining short-range local atomic structure.[17] From a practical standpoint, both α-U and α-Pu are difficult to prepare in macroscopic single-crystal form. EXAFS is attractive as a technique for these materials since long-range order is not required for high-quality EXAFS results. In addition, we use EXAFS to track the vibrational properties of individual bonds in the material as a function of temperature. Bonds of different lengths that can be resolved in the Fourier transform (FT) of the high-resolution EXAFS data can be monitored independently versus temperature. In this paper we report the results of high-resolution EXAFS measurements on α-Pu and α-U samples, and the results of fits of structural models to the EXAFS data, from which detailed short-range structural and bond vibrational information about these two phases is determined. This information about the local structural environment is complementary to long-range structural information determined from previous XRD and neutron diffraction measurements on these systems.[1,2,7–14] To our knowledge there are no previous detailed EXAFS experiments on the structure of α-U and the low-temperature CDW modulation in the literature. Using EXAFS to investigate the bond lengths and detailed short-range structure of α-U will help clarify the nature of the CDW dislocation wave. In particular, our measurement of the CDW using EXAFS is the first observation of the structure of the CDW in polycrystalline α-U. Earlier measurements using XRD or neutron scattering require carefully prepared single-crystal samples.[2,7–14] Heat capacity (C_p) measurements of the CDW in polycrystalline α-U have been

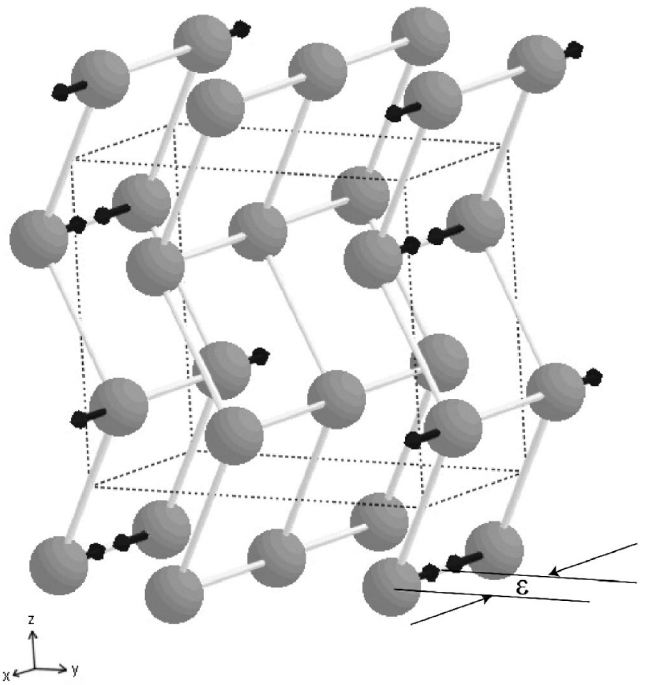

FIG. 2. Atomic structure of orthorhombic α-U. $a=2.854$ Å, $b=5.870$ Å, $c=4.956$ Å (from Ref. 2). The unmodified unit cell is shown. Black arrows indicate the directions of atomic displacements for the charge density wave (CDW), which doubles the unit cell along the (100) direction. ε is the atomic displacement of the CDW along (100), and its magnitude in the figure is much larger than the actual value. The bond lengths along the displacements are shortened and lengthened to $2.84\pm\Delta R$, where $\Delta R=2\varepsilon$.

made.[18,19] While the $T=43$ K structural transition is observed in polycrystalline samples, the 22 K transition is only observed as a very slight feature in the C_p vs T curve, and the 37 K transition has not been observed. All three transitions are clearly observed in heat capacity measurements of single-crystal and "pseudo"-single-crystal α-U samples.[19–21] In polycrystalline samples, the anisotropic thermal expansion of each α-U grain is restrained by intergrain forces due to the orientation mismatch between adjacent grains. This restraint reduces the effects of the CDW on thermal expansion, specific heat, and electronic transport measurements of polycrystalline α-U samples.[14,22] The EXAFS measurement averages the local structure over all atoms in the sample, and is independent of the presence or absence of long-range ordering. The CDW-modulated structural contribution inside each grain will contribute constructively to the overall EXAFS signal for polycrystalline α-U. The grain size of our sample sets an upper limit on the coherence length required to form the CDW in α-U. Additionally, by measuring the U-U bond length distributions with EXAFS, the amplitude of the CDW and the extent of its "squaring" can be investigated further.

In the case of Pu, while several groups studied fcc δ-Pu with EXAFS,[23–27] and recently Wong *et al.* mapped out the phonon density of states for a Ga-doped δ-Pu alloy,[28] there are only two EXAFS studies related to α-Pu. Espinosa *et al.*[29] determined the local structure of α-Pu in zone-refined, 32-year-old aged, and Ce-doped α-Pu samples at a fixed temperature, and observed changes in the disorder of the first Pu-Pu coordination shell with doping and aging. In the present work we extend the α-Pu structure determination to higher spatial resolution (longer EXAFS k-range) and examine the temperature dependence of the EXAFS. The results are compared to our group's previous study of a mixed phase 1.9 at. % Ga-doped alloy,[30] in which the local structure and correlated Debye temperatures of the Ga-containing α'-Pu and δ-Pu phases were separated in the fits to the temperature-dependent EXAFS. The α'-Pu phase consists of Ga atoms "trapped" in a metastable α-Pu structure. In this earlier study, the α'-Pu phase formed in platelets through martensitic transformation upon quenching to 148 K, and amounted to 30 wt. % of the sample, compared to the pure α-Pu sample examined here.

The outline of the paper is as follows. In Sect. II we discuss the details of sample preparation and EXAFS experimental setup and data analysis. In Sect. III we present the L_{III}-edge EXAFS data for α-Pu and α-U. These data include both k-space and R-space (FT) representations of low-temperature, high-resolution EXAFS spectra and a series of lower-resolution EXAFS spectra as a function of temperature. In Sect. III we also describe the curve-fitting analysis procedure and results of curve-fitting analysis, as well as the fits of the correlated Debye model to the temperature dependence of the EXAFS Debye-Waller factors. In Sect. IV we discuss the results in the context of the local atomic structure and the vibrational properties of bonding in the α-Pu and α-U phases, compare the results to earlier Debye temperature measurements, as well as describe the nature of the α-U CDW. Lastly, in Sect. V we present our conclusions.

II. EXPERIMENTAL DETAILS

A. Sample preparation

All samples were prepared at Lawrence Livermore National Laboratory (LLNL) using bulk α-Pu from a batch of ^{239}Pu metal, and bulk α-U from a batch of depleted U (mostly ^{238}U) metal. Bulk metal pieces were thinned to $\sim$14 μm in a series of sawing, lapping, and mechanical polishing steps, in order to achieve the desired thickness for EXAFS transmission measurements. Lastly, electropolishing reduced the final foil thickness to 8–10 μm, and also removed any accumulated oxide material from the surface. All sample preparation was done in an inert argon atmosphere glove box. The samples were encapsulated under argon using a specially designed, triple containment x-ray compatible cell, as described elsewhere.[26] The samples remained in this containment cell during shipment to and from Stanford Synchrotron Radiation Laboratory (SSRL) and throughout the EXAFS experiment. The α-U sample contains a few wt. % UO_2, as verified by Cu Kα x-ray diffraction (XRD) measurements in air performed at LLNL several months after the EXAFS experiment. Only the α-U and UO_2 phases were observed using XRD, and the few wt. % UO_2 was most likely formed due to surface oxidation in air after the sample was removed from triple containment. The α-Pu sample is also expected to have phase purity and oxide concentration similar to the α-U sample, since the α phase is the room-temperature phase of pure Pu. The triple-contained sample was mounted in an open cycle liquid helium flow cryostat for variable temperature EXAFS measurements. Temperature measurement errors are within $\sim$1 K, and are stable to within $\sim$0.2 K. EXAFS measurements began $\sim$20 days after preparation and encapsulation of the samples at LLNL.

B. EXAFS data acquisition

Plutonium and uranium L_{III}-edge x-ray absorption spectra were collected at SSRL on the wiggler side station beamline 4-1 under normal ring operating conditions using a Si (220), half-tuned, double-crystal monochromator operating in the unfocused mode. The vertical slit height inside the x-ray hutch was set at 0.5 mm for both the α-Pu and the α-U samples. The horizontal slit widths were 0.85 mm and 0.75 mm for the α-Pu and α-U samples, respectively, which is smaller than the diameter of the samples (2.8 mm). Pu and U L_{III}-edge spectra were measured in the transmission mode using Ar-filled ionization chambers for the incident and transmitted x rays. The x-ray absorption spectra of triple-contained oxide reference powders (PuO_2 and UO_2) were measured in the transmission mode simultaneously to the metal samples for energy calibration.

III. EXAFS RESULTS

A. Raw data treatment

XAFS raw data treatment, including calibration, normalization, and subsequent processing of the EXAFS and XANES (x-ray absorption near-edge structure) spectral regions was performed by standard methods reviewed

TABLE I. Coordination numbers N_i and Pu-Pu bond length distributions R_i for each of the eight inequivalent sites in the α-Pu unit cell calculated from the diffraction results of Ref. 1, as well as the site-averaged values. The first four shells of the fit to the high-resolution EXAFS data are included. Note that bond lengths also exist in the ranges 4.20 Å–4.77 Å and 4.88 Å–5.42 Å, but the bond length distribution is much more dispersed than in the third and fourth shell ranges specified.

Site	N_1	R_1 range	N_2	R_2 range	N_3	R_3 range	N_4	R_4 range
Pu1	5	2.57 Å–2.76 Å	7	3.20 Å–3.71 Å	8	4.79 Å–4.84 Å	10	5.46 Å–5.57 Å
Pu2	4	2.60 Å–2.64 Å	10	3.19 Å–3.61 Å	4	4.78 Å–4.86 Å	7	5.42 Å–5.57 Å
Pu3	4	2.58 Å–2.66 Å	10	3.24 Å–3.65 Å	6	4.78 Å–4.84 Å	6	5.44 Å–5.48 Å
Pu4	4	2.58 Å–2.74 Å	10	3.26 Å–3.41 Å	10	4.78 Å–4.86 Å	6	5.42 Å–5.49 Å
Pu5	4	2.58 Å–2.72 Å	10	3.24 Å–3.51 Å	7	4.78 Å–4.86 Å	5	5.47 Å–5.54 Å
Pu6	4	2.63 Å–2.74 Å	10	3.20 Å–3.65 Å	2	4.82 Å–4.82 Å	6	5.49 Å–5.57 Å
Pu7	4	2.57 Å–2.79 Å	10	3.30 Å–3.51 Å	5	4.78 Å–4.86 Å	9	5.44 Å–5.57 Å
Pu8	3	2.76 Å–2.79 Å	13	3.19 Å–3.71 Å	4	4.80 Å–4.82 Å	7	5.47 Å–5.57 Å
Average	4	2.57 Å–2.79 Å	10	3.19 Å–3.71 Å	5.75	4.78 Å–4.87 Å	7	5.42 Å–5.57 Å

elsewhere[31,32] using the EXAFSPAK suite of programs developed by George of SSRL. Typically, at each temperature two Pu or U transmission XAFS scans were collected from each sample and the results were averaged. The energies of the first inflection points for the oxide reference powder absorption edges, E_r, were calibrated to 18 053.1 eV (Pu L_{III}) and 17 166.0 eV (U L_{III}), and the energies of the simultaneously measured sample spectra were shifted accordingly. The EXAFS amplitudes were normalized relative to the smoothly varying absorption background $\mu_0(E)$. The background optimization code AUTOBK[33] was used to fit μ_0(E) using a piecewise spline that minimizes the spectral weight of the EXAFS real-space Fourier transform (FT) below $R_{\mathrm{bkg}} < 1.9$ Å.

B. High-resolution EXAFS data and fitting results

1. α-Pu

Nonlinear least squares curve fitting was performed on the k^3-weighted data using the EXAFSPAK program OPT. Theoretical phase and amplitude functions were calculated from the program FEFF8.1 developed by Rehr *et al.*[34,35] All of the Pu-Pu interactions were modeled using single scattering (SS) paths whose lengths were derived from the monoclinic α-Pu model structure determined from x-ray diffraction, with $a = 6.183$ Å, $b = 4.822$ Å, $c = 10.963$ Å, and $\beta = 101.79$ deg[1]. Table I lists the bond length distributions of the first four shells for each of the eight inequivalent sites in the α-Pu structure, as determined by XRD, as well as the site-averaged distributions used in the fit to the α-Pu EXAFS. The amplitude reduction factor S_0^2 was fixed at a value of 0.55 for Pu, as determined from our previous EXAFS measurements of 1.9 at. % and 3.3 at. % Ga-doped Pu samples.[26,30] The energy shift ΔE_0 was first varied for each of the spectra in the α-Pu dataset, and then ΔE_0 was fixed at the average value of −18.3 eV for all spectra in the final fit.

Figure 3(a) displays the Pu L_{III}-edge EXAFS data and best fit, while Fig. 3(b) displays their FT's, for the α-Pu sample, measured at temperature $T = 10$ K. These EXAFS were transformed over a k range of $k \in [2.4\ \text{Å}^{-1}, 21.3\ \text{Å}^{-1}]$, resulting in a real-space resolution of ~0.09 Å. The breakdown of the FT of the α-Pu low-temperature fit into subshell components also is shown in Fig. 3(b). The measured bond lengths of the EXAFS FT peaks are consistent with the average bond lengths of the distributions in each shell of the α-Pu structure listed in Table I.

At this resolution, the splitting of the first and second neighbor shells into shorter and longer bond lengths is observed (Fig. 3(b)). Since the bond length distribution is over a range of values averaged over all eight Pu sites in the unit cell, the total of the subshell coordination numbers was fixed to be equal to the site-averaged coordination number for the entire shell, i.e., $N_1 = N_{1a} + N_{1b} = 4$ and $N_2 = N_{2a} + N_{2b} = 10$, but N_{1a} and N_{2a} were varied. In addition, the Debye-Waller factors of the two subshells were linked to be equal to one another, i.e., $\sigma_{1a}^2 = \sigma_{1b}^2$ and $\sigma_{2a}^2 = \sigma_{2b}^2$. The best fit to the data results in the first two subshells splitting equally, $N_{1a} = N_{1b} = 2.00 \pm 0.05$, with a bond-length splitting of $R_{1b} - R_{1a} = 0.098 \pm 0.002$ Å. The second shell bond length is weighted slightly more toward longer bond lengths, $N_{2b} = 5.5 > 4.5 = N_{2a}$, with a larger splitting of $R_{2b} - R_{2a} = 0.153 \pm 0.002$ Å. The coordination numbers of the third and fourth shells were fixed to their site-averaged values of 5.75 and 7.0, respectively. By comparing the total FT magnitude of the data to the magnitudes of the subshell components, it is seen that the 0.10 Å splitting between the first shell components results in largely destructive interference, while the 0.15 Å splitting between the second shell components results in mostly constructive interference. The destructive interference in the first shell is not seen in the α-Pu EXAFS FT of the earlier α-Pu EXAFS study.[29] This is because a shorter EXAFS k range $k \in [3.4\ \text{Å}^{-1}, 12.8\ \text{Å}^{-1}]$ is used in the earlier study, resulting in worsened spatial resolution of the EXAFS FT. Our α-Pu EXAFS data transformed over a similar k range to Ref. 29 results in a similar FT, with more constructive interference in the first shell FT peak.

2. α-U

The U-U interactions were modeled using the structure of orthorhombic α-U determined from XRD, with a

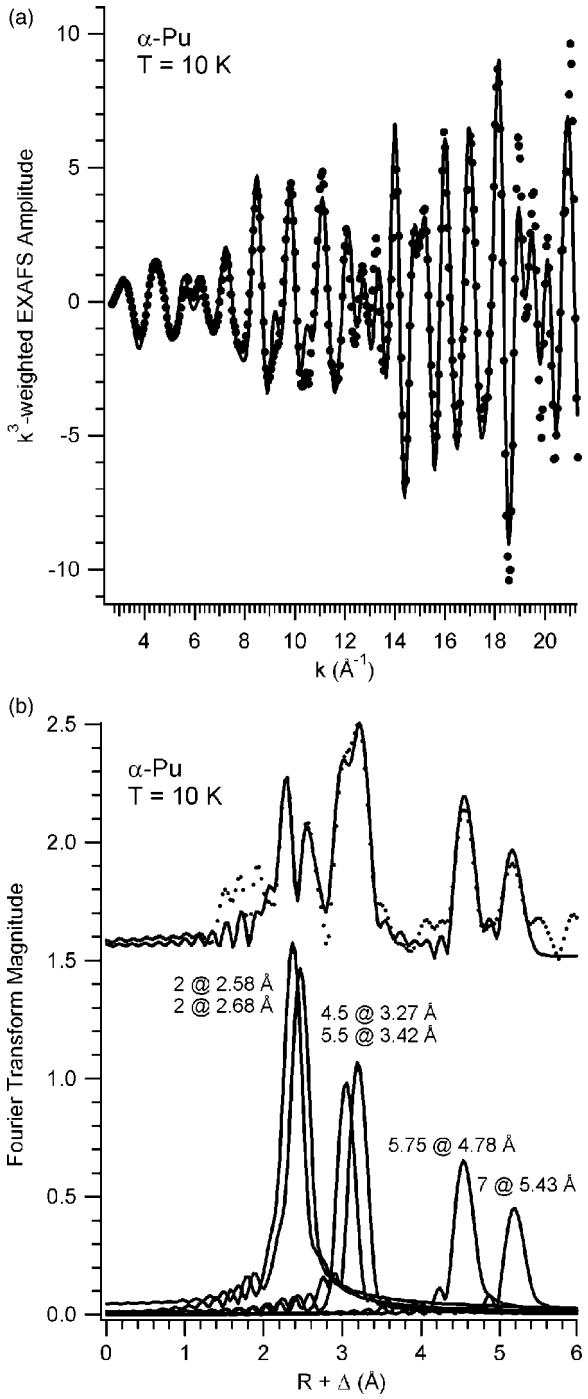

FIG. 3. (a) Pu L_{III}-edge k^3-weighted transmission EXAFS data (points) and best fit (solid line) for α-Pu at $T=10$ K. Note that the disagreement between the data and the fit in k space mostly is due to contributions to the data from longer pair distances than were included in the fit, i.e., shells with pair distances $R>6.0$ Å. (This same situation exists in Figs. 4(a) and 5(a).) (b) Fourier transforms (FT's) of the Pu L_{III} EXAFS data (points) and best fit (solid line) for the α-Pu sample at $T=10$ K. High-resolution FT's were taken over the k^3-weighted EXAFS over the k range $k\in[2.7\ \text{Å}^{-1},21.3\ \text{Å}^{-1}]$. The six components of the fit also are displayed. The first and second shells of α-Pu each are split into two subshells. Note the destructive interference in the first shell and the constructive interference in the second shell of the EXAFS data.

TABLE II. Coordination numbers N_i and U-U bond lengths R_i, and bond direction cosines X_i/R_i along the a direction for the single crystallographic site in the α-U unit cell calculated from the diffraction results of Ref. 2. The first six shells are included, corresponding to the shells used in the high-resolution EXAFS fits. Asterisks mark paths for which the path direction cosine along the a direction $X_i/R_i\geqslant 0.5$, i.e. paths pointing mostly in the direction of the (100) soft phonon and charge density wave.

Shell i	Coordination Number N_i	Bond length R_i	Projection along (100) X_i/R_i
1*a*	2	2.73	0.00
1*b*	2	2.84	1.00*
2*a*	4	3.26	0.44
2*b*	4	3.34	0.43
3	4	3.95	0.72*
4*a*	2	4.94	0.00
4*b*	4	5.01	0.28
4*c*	4	5.17	0.82*
4*d*	4	5.22	0.82*
4*e*	2	5.28	0.00
5*a*	2	5.67	1.00*
5*b*	4	5.69	0.50*
6*a*	2	5.87	0.00
6*b*	8	5.91	0.24
6*c*	4	6.00	0.47

$=2.854$ Å, $b=5.870$ Å, $c=4.956$ Å,[2] and includes only SS paths, with the exception of the collinear multiple-scattering (MS) path along (100) with length $R=2a=5.67$ Å. Table II lists all of the FEFF paths used for the fit of the unmodulated α-U structure to the EXAFS data, along with their coordination number and direction cosine along (100). The energy shift ΔE_0 was first varied for each of the spectra in the α-U dataset, and then ΔE_0 was fixed at the average value of +4.7 eV for all spectra in the final fit. S_0^2 for α-*U* also was varied in a preliminary run and then fixed at the average value of 0.9 for the final fits.

Figure 4(a) displays the corresponding U L_{III}-edge EXAFS data and best fit for the α-U sample, while Fig. 4(b) displays their FT's, measured at temperature $T=55$ K. These EXAFS were transformed over a k range of $k\in[2.7\ \text{Å}^{-1},20.5\ \text{Å}^{-1}]$, resulting in a real-space resolution similar to that of the FT of the α-Pu data ($\sim$0.09 Å). The breakdown of the FT of the α-U low-temperature fit into subshell components is also shown in Fig. 4(b). For data at both $T=11$ K and $T=55$ K, neighboring atomic shell contributions out to $R=6.0$ Å are included in the fit, and the distances and Debye-Waller factors of each shell are allowed to vary. The $R_{1a}=2.73$ Å bond is assigned a coordination number of $N_{1a}=2$, while the shells at 3.28 Å, 3.93 Å, 4.99 Å, 5.21 Å, and 5.99 Å have coordination numbers $N_2=8, N_3=4, N_{4a}=6, N_{4b}=10$, and $N_{5b}=10$, respectively, in order to represent the α-U structure of Table II. The coordination number of the shell at $R_{5a}=5.64$ Å is allowed to vary, because this shell also includes multiple scattering contributions, since it is twice the 2.84 Å bond length along the (100)

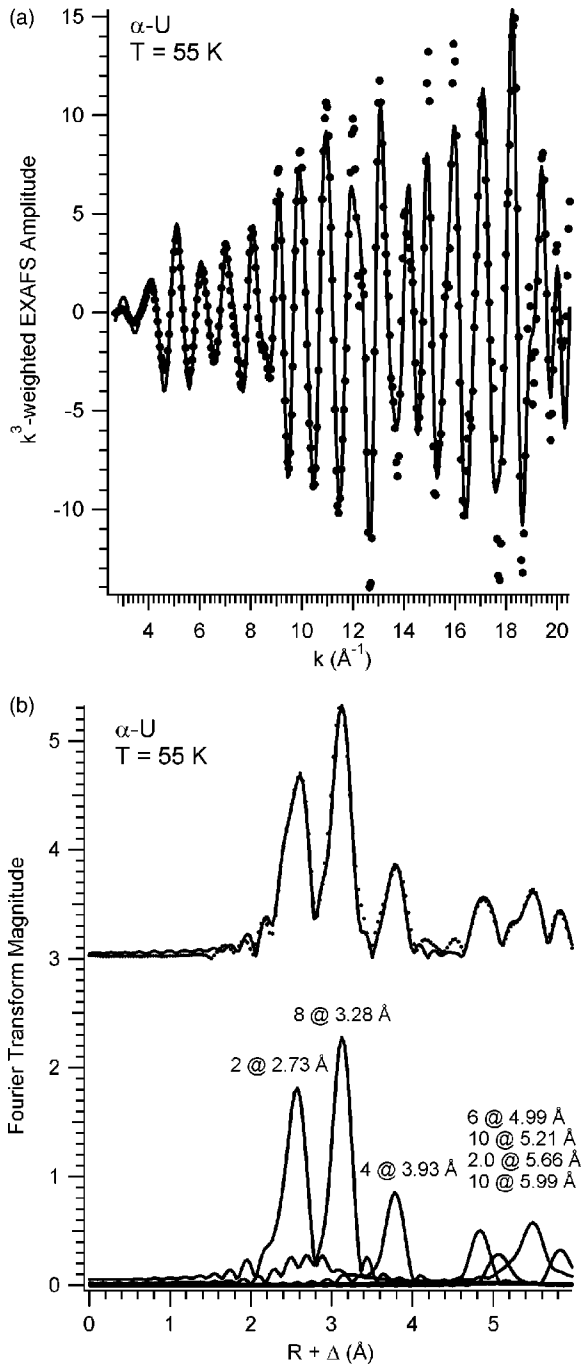

FIG. 4. (a) U L_{III}-edge k^3-weighted transmission EXAFS data (points) and best fit (solid line) for α-U at $T=55$ K. The fit includes all shells with pair distances less than $R=6.0$ Å. (b) U L_{III} EXAFS FT data (points), fit (solid line), and fit components for the α-U sample at $T=55$ K. High-resolution FT's were taken over the k^3-weighted EXAFS over the k range $k\in[2.7\ \text{Å}^{-1}, 20.5\ \text{Å}^{-1}]$.

direction. The FT peak positions correspond well to the expected positions of the shells in the unmodified α-U structure listed in Table II, with the exception of the first shell, which is shortened to 2.73 Å from an expected mixture of two bonds at $R=2.73$ Å and two bonds at $R=2.84$ Å.

As seen from Table II, the first and second shells should be split in the unmodulated α-U geometry, with splittings of $R_{1b}-R_{1a}=0.11$ Å and $R_{2b}-R_{2a}=0.08$ Å, respectively. The first and second shell bond lengths in unmodulated α-U each are evenly split between two well-defined bond lengths, and the bond length distribution is the same for every U atom in the unit cell, unlike the case of α-Pu. With this well-defined structure and the high resolution ($\sim$0.09 Å) of the data, one would expect to resolve the splittings in the first and second shell in the low-temperature EXAFS FT for an unmodulated α-U structure, or at least see destructive interference effects as in the case of the first shell splitting of α-Pu. Contrary to this expectation, the first two shells each have a strong single peak in the α-U FT, even at the highest resolution, rather than the interference between subshells resolved in the case of α-Pu. The lack of a first shell splitting can be attributed to the lack of an $R=2.85$ Å component in the EXAFS at and above $T=55$ K. As seen in Table II, the $R=2.85$ Å bonds are directed along the (100) direction, parallel to the direction of the "optical" displacement of U atoms in the $\mathbf{q}\approx(0.5,0,0)$ soft phonon observed in α-U. This phonon has a significant amplitude and low frequency even at temperatures of $T=55$ K, so we expect that the Debye-Waller factor for these $R=2.85$ Å bonds is increased dramatically due to the anticorrelated motion of the U-U bond modulated by the population of this optical phonon. The two bonds at $R=2.85$ Å are assumed to have a large enough Debye-Waller factor so that they have a minimal contribution to the EXAFS FT at and above $T=55$ K.

The low-temperature CDW-distorted α-U phase was modeled using the commensurate model of Smith *et al.*,[8] which includes an "optical" distortion of neighboring atoms and a doubling of the lattice parameter a along the (100) direction. The shortest U-U bonds (shell 1a) are in the $\langle 100\rangle$ plane with bond length $R_{1a}=2.73$ Å. These bonds are not affected by the CDW. The two nearest neighbor bonds along (100) (shell 1b) have a single bond length of $R_{1b}=2.84$ Å in the unmodulated structure. This single bond length is dispersed into a range of bond lengths by the CDW. The maximum amplitude of the individual atom CDW displacements is ε, which results in bond lengths ranging from $2.84\ \text{Å}-\Delta R$ to $2.84+\Delta R$, where $\Delta R=2\varepsilon$. The distribution of the bond lengths can be modeled as a square wave (one bond at $2.84\ \text{Å}-\Delta R$ and one bond at $2.84\ \text{Å}+\Delta R$) or a sine wave, which also has bond lengths at intermediate values. Although the CDW has been shown to be incommensurate in terms of its long-range order, EXAFS is sensitive only to short-range interactions and bond lengths and not long-range ordering. Therefore the commensurate model provides a good starting point for the expected U-U bond lengths in this phase, and the near-neighbor bond length distributions do not depend on this long-range structure.

Figure 5(a) displays the U L_{III}-edge EXAFS data and best fit for the α-U sample, while Fig. 5(b) displays their high-resolution FT's, at the lowest measured temperature T $=11$ K. As with the $T=55$ K data, the $T=11$ K EXAFS data were transformed over a k range of $k\in[2.7\ \text{Å}^{-1}, 20.5\ \text{Å}^{-1}]$. For the $T=11$ K fit, two additional components are added to represent the CDW-modulated bonds, as described below.

Comparing the FT's of Figs. 4(b) and 5(b), a large increase in the amplitude of the first shell FT peak is seen in the $T=11$ K data, while the rest of the $T=11$ K FT is similar

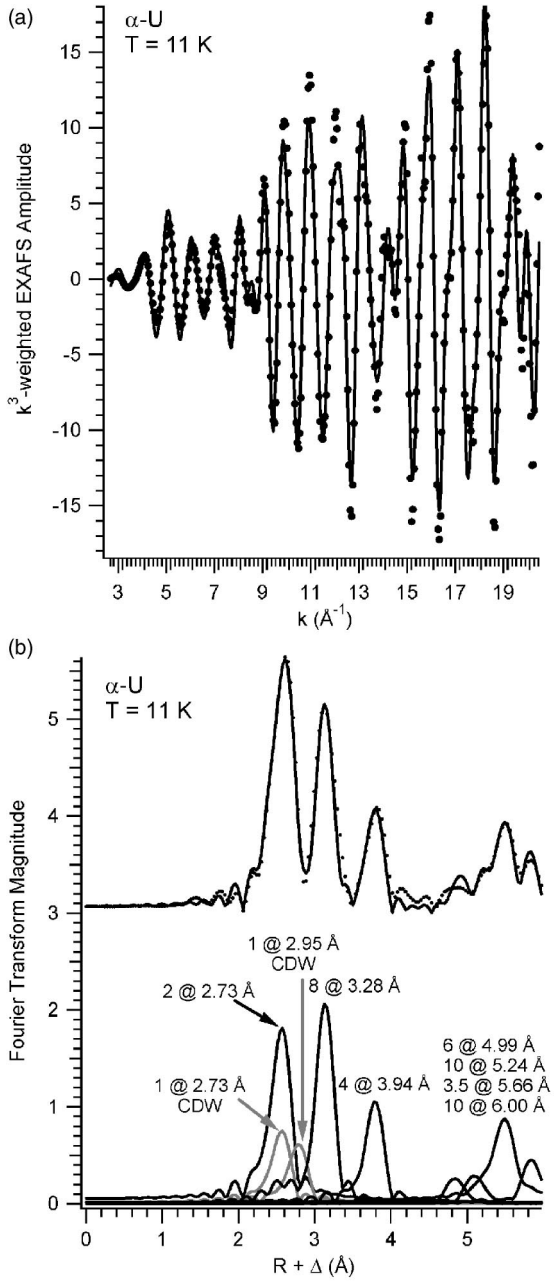

FIG. 5. (a) U L_{III}-edge k^3-weighted transmission EXAFS data (points) and best fit (solid line) for α-U at $T=11$ K. The fit includes all shells with pair distances less than $R=6.0$ Å. (b) Fourier transforms (FT's) of the U L_{III} EXAFS data (points) for the α-U sample at $T=11$ K, along with the FT's of the fits (solid line) to the data. High-resolution FT's were taken over the k^3-weighted EXAFS over the k range $k\in[2.7\ \text{Å}^{-1}, 20.5\ \text{Å}^{-1}]$. The nine components of the fit also are displayed. The effect of the CDW modulation is modeled by a square wave distribution with one bond each at $R=2.84\ \text{Å}\pm\Delta R$ where $\Delta R=0.11$ Å (gray lines).

to the $T=55$ K data. The large change in the overall lineshape of the FT cannot be attributed to normal thermal Debye-Waller effects, which would show little change in the Debye-Waller factor over the temperature range from $T=11$ K to $T=55$ K. Instead, the dramatic change in the α-U EXAFS over this temperature range can be attributed to a change in the local structure of the first and second shells of α-U at $T=11\ \text{K} < T_{\mathrm{CDW}}$ relative to the unmodulated structure at $T=55\ \text{K} > \mathrm{T_{CDW}}$. A CDW modulation of the 2.84 Å bond along (100) can be modeled as a square wave distribution (one bond at $2.84\ \text{Å}-\Delta R$ and one bond at $2.84\ \text{Å}+\Delta R$) or as a sine wave distribution, which has additional bond lengths at intermediate values. Figure 5(b) shows the component breakdown of the fit to the $T=11$ K EXAFS FT of α-U. This fit is very similar to the fit of the $T=55$ K data of Fig. 4, except for the addition of two additional components corresponding to the CDW-shortened and CDW-lengthened bonds at $R=2.73$ Å and $R=2.95$ Å. In the fit to the $T=11$ K data, the coordination numbers of these components were fixed at $N_{1b}=N_{1c}=1$, the distances were constrained to have an average value of $(R_{1a}+R_{1b})/2=2.84$ Å, and the Debye-Waller factors were set equal, i.e. $\sigma^2_{1b}=\sigma^2_{1c}$.

The main difference between the EXAFS above and below $T_{\mathrm{CDW}}=43$ K is fit well by the square-wave CDW model. A similar fit at $T=11$ K replacing the two CDW bond lengths at $R=2.84\ \text{Å}\pm\Delta R$ by two bonds both at the unmodulated α-U bond length $R=2.84$ Å (i.e., setting $\Delta R=0$) resulted in the fit program giving these two bonds a very high Debye-Waller factor (0.030 Å^2) with very little contribution to the EXAFS. Due to poor agreement with the contribution of first shell to the $T=11$ K EXAFS data, the unmodulated α-U model structure results in a poorer fit to the data than the structure modulated by the square-wave CDW. In addition, the fit to the lower-resolution $T=11$ K, 25 K, and 35 K data is significantly improved by adding the CDW components, as determined by the degree of improvement in the reduced χ^2 of the fits before and after adding the additional components. The ratio of the reduced χ^2 needs to be larger than $1+2^{*}\mathrm{sqrt}(2/v)$, where $v=16.6$ is the number of degrees of freedom for these fits. For the fits at $T=40$ K and 45 K, the improvement in reduced χ^2 is equal to this significance limit, while it is slightly lower than this for higher temperatures.

Comparing the $1/R^2$-weighted bond length distribution of the unmodulated α-U structure of Ref. 2 and the square-wave CDW-modulated α-U structure of Ref. 8 to the EXAFS data FT at $T=11$ K from the α-U sample (not shown), we find that the amplitude of the first shell FT peak of the data at $R=2.73$ Å is significantly higher than expected for the bond length distribution for unmodulated α-U. The agreement is greatly improved when the α-U EXAFS data FT is compared to the bond length distribution for the CDW-modulated α-U structure.

3. α-U EXAFS temperature series

Figure 6 shows the temperature series of the high-resolution U L_{III}-edge EXAFS data FT of the α-U sample for temperatures from $T=10$ K to 130 K. The k range over which the FT's are taken is $k\in[2.7\ \text{Å}^{-1}, 20.5\ \text{Å}^{-1}]$. Unlike the case of α-Pu, the overall shape of the FT changes dramatically below $T=55$ K for α-U. In particular, the magnitude of the peaks labeled "A" decrease with temperature while the "B" peaks increase until a maximum at $T=55$ K and then decrease with temperature. As a result, the first neighbor (A1) peak magnitude is slightly larger than that of the second neighbor (B2) peak at $T=11$ K, while at T

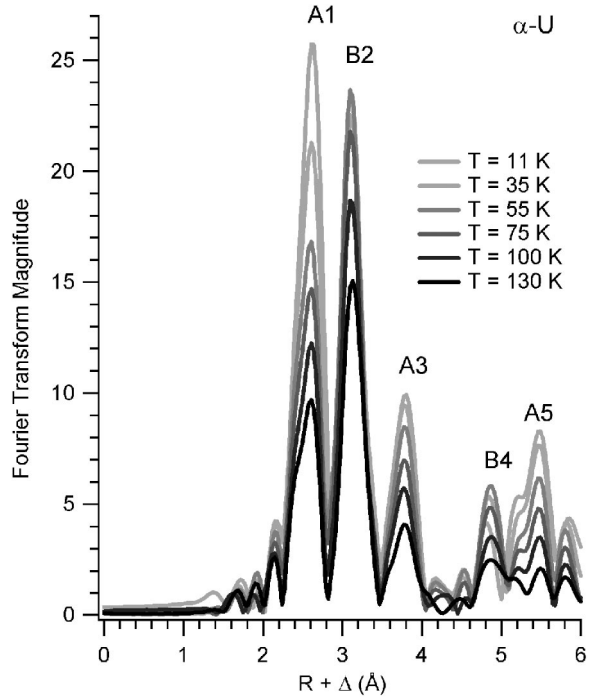

FIG. 6. High-resolution overlay plot of the EXAFS FT's of the α-U sample as a function of temperature. FT's are taken over the k range $k \in [2.7\ \text{Å}^{-1}, 20.5\ \text{Å}^{-1}]$, while the temperature range is limited to a maximum temperature of 130 K. Note that the α-U EXAFS FT has peaks with differing temperature dependencies. The peaks have been labeled group "A" and group "B" according to their temperature dependence and direction relative to (100), and are discussed in the text.

$=55$ K the A1 peak is only ~60% of the B2 peak. Above $T=55$ K, no further changes in the relative intensities of the FT components lineshape occur, and typical Debye-Waller damping continues to broaden all of the peaks at a similar rate. At $T=55$ K and above, the overall lineshape is more similar to the $1/R^2$-weighted bond length distribution for unmodulated α-U (not shown). The variation of the k-space EXAFS with temperature (not shown) has a similar behavior to the FT's. We attribute the anomalous behavior of the EXAFS at temperatures below $T=55$ K to structural changes resulting from the CDW-modulated α-U phase.

The different thermal behavior of the "A" and "B" peaks in the α-U EXAFS FT's of Fig. 6 is related to the directions of the near-neighbor paths contributing to each peak. The "A" peaks consist of bonds or atom-to-atom paths directed primarily along the a or (100) direction. From Table II, bonds contributing to the A1 and A5 peaks have a direction cosine along a equal to $X/R=1$ and points entirely along the (100) direction, while the A3 peak consists of paths primarily along the (100) direction with $X/R=0.72$. In contrast, the "B" peaks consist of paths which either have an intermediate component along a (the B2 peak has $X/R=0.44$) or are a mixture of two types of bonds with different directionality (the bonds in the B4 region include 8 bonds with $X/R \leqslant 0.28$ and 8 bonds with $X/R=0.82$). The CDW displacement direction is primarily along the (100) direction, as is the soft phonon wave vector. Both the spread in the bond length distribution produced by the CDW displacement wave and the larger thermal vibrational amplitude of the soft phonons will act to rapidly increase the Debye-Waller factor of bonds pointing primarily along the (100) direction, while bonds oriented more in the $\langle 100 \rangle$ plane will be affected less by the CDW displacements and soft phonon thermal vibrations. The different thermal behavior of the various shell components of the high-resolution EXAFS FT is evidence of the anisotropy of the α-U CDW and soft phonon.

Determining this anisotropy is dependent upon high-resolution EXAFS data as well as tracking its detailed thermal dependence over a range of temperature values. The EXAFS technique can separate the thermal behavior of bonds in different directions due to the difference in bond lengths for bonds along different directions in the α-U structure. This anisotropy is local to each atom in α-U, so it can be detected by a local probe such as EXAFS, and is not affected by the relative orientation of crystallites in the sample. The CDW changes this local structure and therefore is observable with EXAFS, without needing long-range order in the sample, as do the diffraction and scattering experiments.

C. Vibrational analysis

For both α-Pu and α-U, we fit a local structural model to all data from $T=10$ K to room temperature using a consistent fitting procedure. The k ranges used for the EXAFS temperature studies were $[2.7\ \text{Å}^{-1}, 13.4\ \text{Å}^{-1}]$ for Pu and $[2.7\ \text{Å}^{-1}, 14.8\ \text{Å}^{-1}]$ for U. These k ranges are shortened from the low-temperature fits in order to keep the range consistent at all temperature values. The usable k range of the EXAFS is intrinsically shortened by Debye-Waller damping at higher temperatures. This smaller k range results in a reduction of the resolution of the EXAFS FT in R space. The EXAFS data are weighted by a factor of k^3 for the fits and for plotting the data and their FT's. After determining the Fourier Transform (FT) of the EXAFS over the specified k range with a step-function window, the EXAFS FT was back-transformed over the bond-length range of interest, i.e. $R \in [1.3\ \text{Å}, 4.1\ \text{Å}]$ for α-Pu and $R \in [1.9\ \text{Å}, 4.1\ \text{Å}]$ for α-U, which corresponds to the first and second atomic shells of α-Pu, and the first through third shells of α-U. The fits were made to the back-transformed filtered data.

We analyzed the high-resolution datasets at low temperature first to establish the correct modeling parameters for the neighboring atomic shells in the thermal analysis. We confine our data to the first two shells in α-Pu and the first three shells in α-U by appropriately filtering the data in R space. For α-Pu, the bond distances and the Debye-Waller factors for each of the two shells are varied, for a total of four variables in each fit. For α-U, the third shell is included to better fit the destructive interference that occurs near $R+\Delta = 3.5$ Å in the FT. The bond distance and the Debye-Waller factor for the third shell also are varied, for a total of six variables in each fit for α-U. In the thermal analysis, S_0^2 and ΔE_0 are fixed to the same values as for the high-resolution fits ($S_0^2=0.55$ and $\Delta E_0=-18.3$ eV for α-Pu; $S_0^2=0.9$ and $\Delta E_0=+4.7$ eV for α-U). Fixing S_0^2 and ΔE_0 avoids correla-

tion problems between S_0^2 and the Debye-Waller factors σ^2, as well as between ΔE_0 and the distances R. Fixing these parameters and the k range ensures a meaningful comparison of values for the distances and Debye-Waller factors at different temperatures in the following thermal Debye analysis.

Figure 7(a) shows the filtered Pu L_{III}-edge EXAFS data of the α-Pu sample as a function of temperature from $T=10$ K to room temperature, along with the best fits to the EXAFS data. The corresponding FT's of the data and fits, are given in Fig. 7(b). The overall shape of the α-Pu EXAFS FT are dampened and broadened by Debye-Waller thermal effects. Similarly, the lower-resolution filtered EXAFS data over the entire temperature range for α-U in Fig. 8(a) are dampened with increasing temperature, as are the corresponding FT's of the data in Fig. 8(b). However, in the case of α-U, there are significant changes in the FT first shell peak intensity relative to the FT second shell peak intensity for $T<55$ K. Above $T=55$ K the changes in the FT lineshape can be explained by normal Debye-Waller thermal effects, and the first and second shell FT peaks are dampened and broadened with temperature at a similar rate.

Tables III and IV list the best fit results for the bond length and Debye-Waller factor of the innermost neighboring atomic shells at each temperature for α-Pu and α-U, respectively. The bond lengths do not change dramatically for either sample over the temperature range, as expected from the small thermal expansion coefficients over this temperature range.[15] This is consistent with our earlier EXAFS study of α'-Pu in a mixed-phase Pu-Ga alloy.[30]

Figures 9(a) and 9(b) display the temperature dependence of the Debye-Waller factors for the first and second shells in α-Pu and α-U, respectively. The lines are the fits of a correlated Debye model[36,37] to the Debye-Waller factor data in the same manner as Refs. 26,30. The correlated Debye model is an extension of the standard Debye model for EXAFS measurements. The same phonon density of states is used in both models. However, unlike the Debye-Waller factor in diffraction measurements, which is proportional to the squared vibrational amplitude of an atom about its equilibrium position, the EXAFS Debye-Waller factor is proportional to the squared vibrational amplitude of the distance between two atoms, each of which are moving about their equilibrium positions. The EXAFS Debye-Waller factor is therefore the sum of the Debye-Waller factors of each of the two atoms about its equilibrium position, plus an interference term due to the degree of correlation between the motions of the two atoms. If the motion of the pair of atoms is correlated, the bond length variation is less than that expected for uncorrelated motion, and the EXAFS Debye-Waller factor is reduced from the individual atom Debye-Waller factor sum. Similarly, anticorrelated motion results in an increased bond length variation and an increased EXAFS Debye-Waller factor. The correlated Debye model includes phonon effects on the increase of the EXAFS Debye-Waller factor with temperature, and accounts for the correlated motion of the atomic pair. Unless otherwise noted in this paper, the phrase "Debye-Waller factor" refers to an EXAFS Debye-Waller factor.

The progression of the Debye-Waller factors for both shells of α-Pu and the second shell of α-U are fit well with the correlated Debye model. However, there is a sharp decrease in the Debye-Waller factor of the first shell of α-U as the temperature is decreased below $T=55$ K. This behavior is due to the dramatic increase in the first shell FT peak magnitude at low temperature, as already seen in the low-temperature α-U EXAFS data of Fig. 6. The low-temperature behavior of the first shell α-U Debye-Waller fac-

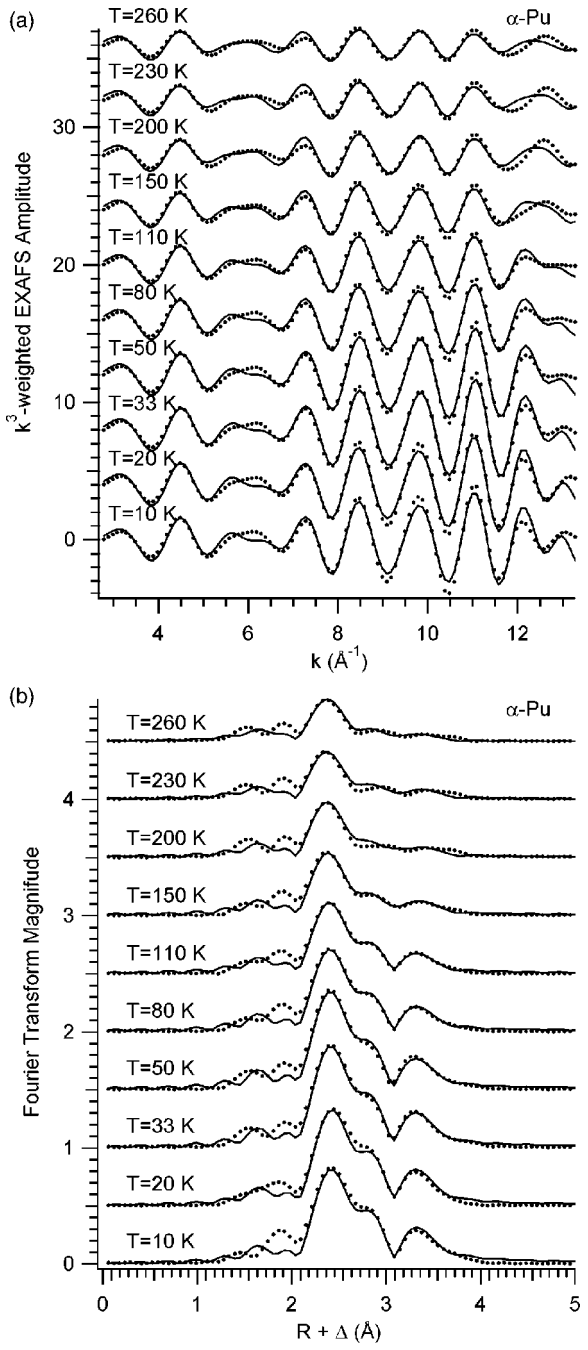

FIG. 7. (a) Fourier-filtered Pu L_{III}-edge k^3-weighted transmission EXAFS data as a function of temperature. Filtering is over the range $R\in[1.3\ \text{Å}, 4.1\ \text{Å}]$. (b) FT's of the EXAFS for the α-Pu sample as a function of temperature. For each plot, the points are the data, and the solid line is the two-shell fit to the data. FT's were taken over the k ranges shown in the upper graph. Note the Debye-Waller damping of the EXAFS with increasing temperature.

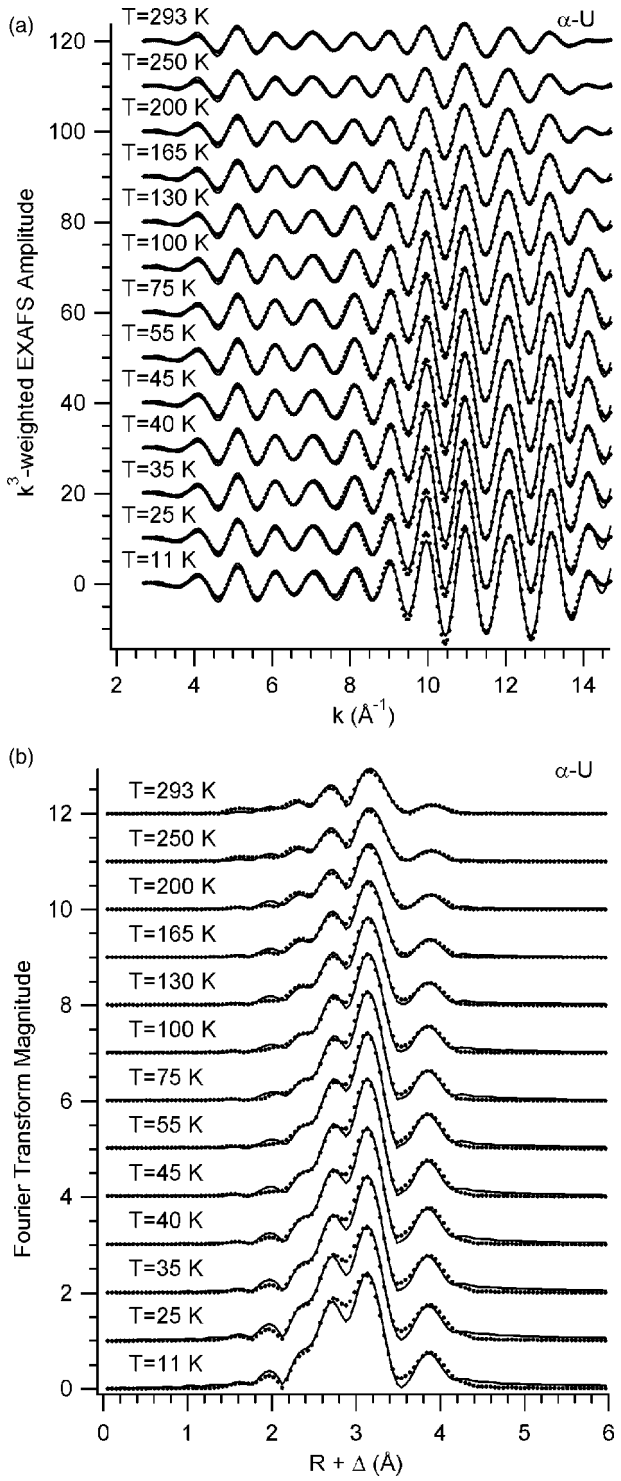

FIG. 8. (a) Fourier-filtered U L_{III}-edge k^3-weighted transmission EXAFS data as a function of temperature. Filtering is over the range $R \in [1.9\ \text{Å}, 4.1\ \text{Å}]$. (b) FT's of the EXAFS for the α-U sample as a function of temperature. For each plot, the points are the data, and the solid line is the three-shell fit to the data. FT's were taken over the k ranges shown in the upper graph. Note the damping of the EXAFS with increasing temperature and the different thermal behavior of the FT's above and below $T_{\mathrm{CDW}} = 43$ K.

tor clearly does not follow the correlated Debye model, for which the Debye-Waller factor is expected to be nearly constant over the temperature range of the anomalous behavior. Therefore this behavior is attributed to a change in the overall structure of the local U environment in α-U at low temperatures, i.e., the existence of the CDW modulation.

Table V lists the correlated Debye temperatures θ_{cD} for the first and second shell bonds in α-Pu and α-U phases, respectively, as determined from the fits of the temperature dependence of the Debye-Waller factors with the correlated Debye model.

IV. DISCUSSION

A. α-Pu Correlated Debye temperature

The correlated Debye temperatures from the temperature-dependent EXAFS data are in good agreement with Debye temperatures from earlier studies. The first shell α-Pu correlated Debye temperature $\theta_{cD}(\alpha\text{-Pu}) = 162 \pm 5$ K is in excellent agreement with the value of 159 ± 13 K for the Ga-containing α'-Pu phase determined in our earlier temperature-dependent EXAFS study of a 1.9 at. % Ga-doped α'-Pu/δ-Pu alloy.[30] Since the force constant of the bond is proportional to the square of the Debye temperature, this result indicates that the strength of the Pu-Pu bond is similar in α-Pu and α'-Pu, and therefore is not influenced dramatically by the presence of Ga in the structure. The correlated Debye temperature of 162 ± 5 K is in the lower end of the range of values reported for α-Pu (153–200 K), as determined by heat capacity measurements.[38–40]

B. α-U Correlated Debye temperature

The correlated Debye model is fit to the temperature dependence of the α-U EXAFS first shell Debye-Waller factor only for temperatures above T_{CDW}, i.e., for $T \geqslant 55$ K. The resulting first shell EXAFS α-U correlated Debye temperature $\theta_{cD}(\alpha\text{-U}) = 199 \pm 3$ K also agrees well with Debye temperatures for polycrystalline α-U from heat capacity measurements (170–207 K).[19–21,39] In addition, our second shell correlated Debye temperature of 195 ± 3 K agrees well with the first shell correlated Debye temperature.

Interestingly, the Debye temperature appears to be a function of grain size in α-U. The Debye temperatures determined from heat capacity measurements for single-crystal and pseudo-single-crystal α-U are 256 ± 0.25 K[21] and 210 ± 4 K,[19] respectively, while our EXAFS measurements on polycrystalline α-U result in $\theta_{cD}(\alpha\text{-U}) = 199 \pm 3$ K. The pseudo-single-crystal sample of Ref. 19 is made up of large mosaic grains of slightly differing orientations. The increase in Debye temperature with a larger grain size is attributed to the removal of constraints on the thermal expansion of α-U caused by grain boundaries.[15] It is interesting to note that while EXAFS probes the local CDW structure within each of the grains, the correlated Debye temperature of the bonds still agrees with that of polycrystalline α-U.[19–21,39]

C. Modeling the α-U CDW

We have defined $\Delta R (= 2\varepsilon)$ as the magnitude of the (100) near-neighbor bond length shift from its non-CDW value of

TABLE III. Temperature-dependent Pu L_{III}-edge EXAFS fitting results. EXAFS data were fitted over the k range [2.7, 13.4 Å^{-1}] by three components: one for nearest neighbor shell and the other two for the second nearest neighbor shell in α-Pu. The coordination numbers were fixed at $N_1=4, N_{2a}=4.65$, and $N_{2b}=5.35 (N_{2a}+N_{2b}=10)$, which is the average value of these coordination numbers in an earlier fit. S_0^2 and ΔE_0 were fixed at 0.55 and −18.3 eV, respectively, and the Debye-Waller factors for the components 2a and 2b were set to be equal, i.e. $\sigma_2^2=\sigma_{2a}^2=\sigma_{2b}^2$.

Sample Temp (K)	Pu-Pu R_1 (Å)[a]	Pu-Pu σ_1^2 (Å^2)[a]	Pu-Pu R_{2a} (Å)[a]	Pu-Pu R_{2b} (Å)[a]	Pu-Pu σ_2^2 (Å^2)[a]
10	2.626	0.004 65	3.268	3.431	0.003 61
20	2.629	0.004 65	3.264	3.429	0.003 84
33	2.621	0.004 33	3.261	3.425	0.003 77
50	2.621	0.004 53	3.264	3.428	0.004 21
80	2.625	0.005 47	3.272	3.434	0.005 11
110	2.622	0.006 34	3.273	3.436	0.006 18
150	2.617	0.007 06	3.289	3.452	0.007 54
200	2.617	0.007 79	3.296	3.462	0.009 58
230	2.621	0.008 72	3.295	3.467	0.009 96
260	2.622	0.009 52	3.286	3.461	0.011 96

[a]Errors in R and σ^2 are estimated to be ±0.005 Å and ±10% based on EXAFS fits of model compounds; cf. Ref. 32.

2.84 Å, i.e. CDW bonds are shifted to $2.84+\Delta R$ and $2.84-\Delta R$ in the square-wave CDW model. Fits to the $T=11$ K data with a square-wave CDW model over a range of ΔR values from 0 to 0.20 Å gave the best fits with physically meaningful Debye-Waller factors with the bond length shifts of $\Delta R=0.07$–0.12 Å. Note that the spread in bond lengths of the first subshells is $2\Delta R$, which is larger than the experimental resolution (~0.09 Å). The two non-CDW bonds at 2.73 Å cannot account for enough intensity to be the entire contribution to the first shell FT peak, and an additional CDW short bond contributes best to this peak when its length is close to 2.73 Å. For values of ΔR less than 0.07 Å, the Debye-Waller factor of the CDW bonds is increased to large values (>0.024 Å^2) indicating little contribution from the CDW component. This is due to the large negative interference between the 2.73 Å EXAFS component and EXAFS components in the vicinity of 2.84 Å. From the values of $\Delta R=0.07$–0.12 Å for the best fits to the $T=11$ K α-U EXAFS data, we derive a magnitude of a square wave CDW displacement of $\varepsilon=\Delta R/2=0.05\pm0.02$ Å. This result is similar to the value of $\varepsilon=0.053\pm0.001$ Å reported in earlier diffraction papers by Marmeggi,[9] although in later papers ε was

TABLE IV. Temperature-dependent U L_{III}-edge EXAFS fitting results. EXAFS data were fitted over the k range [2.7, 14.8 Å^{-1}] by three components for the first three nearest neighbor shells in α-U. The coordination numbers were fixed at $N_1=2, N_2=8$, and $N_3=4$. S_0^2 and ΔE_0 were fixed at 0.9 and +4.8 eV, respectively.

Sample Temp (K)	U-U R_1 (Å)[a]	U-U σ_1^2 (Å^2)[a]	U-U R_2 (Å)[a]	U-U σ_2^2 (Å^2)[a]	U-U R_3 (Å)[a]	U-U σ_3^2 (Å^2)[a]
11	2.725	0.000 78	3.277	0.003 36	3.929	0.003 86
25	2.726	0.000 91	3.277	0.003 41	3.929	0.003 92
35	2.729	0.001 35	3.277	0.003 47	3.929	0.003 85
40	2.731	0.001 54	3.278	0.003 49	3.931	0.003 93
45	2.733	0.001 79	3.277	0.003 48	3.930	0.004 08
55	2.735	0.002 01	3.277	0.003 60	3.928	0.004 20
75	2.737	0.002 32	3.278	0.003 85	3.928	0.004 79
100	2.735	0.002 68	3.279	0.004 25	3.929	0.005 25
130	2.733	0.003 01	3.280	0.004 79	3.932	0.006 00
165	2.732	0.003 49	3.281	0.005 44	3.937	0.007 23
200	2.730	0.004 10	3.282	0.006 19	3.939	0.008 17
250	2.730	0.004 90	3.283	0.007 25	3.941	0.009 78
293	2.730	0.005 69	3.283	0.008 30	3.945	0.011 22

[a]Errors in R and σ^2 are estimated to be ±0.005 Å and ±10% based on EXAFS fits of model compounds; cf. Ref. 32.

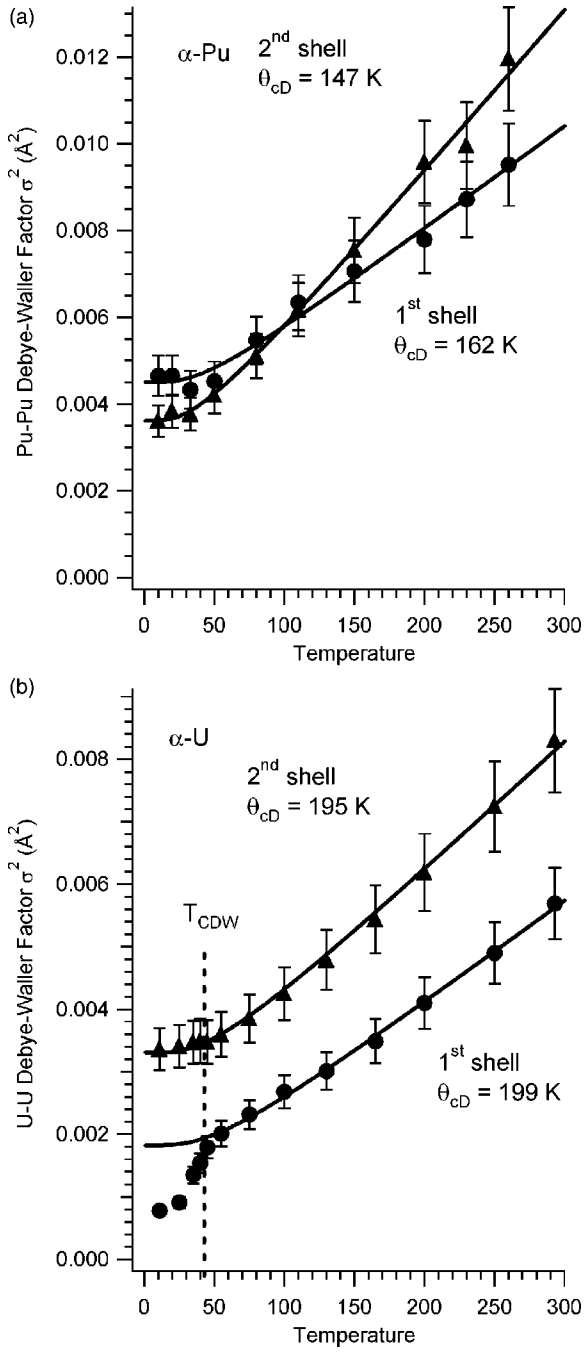

FIG. 9. (a) Plot of the Debye-Waller factor versus temperature for the first and second shell Pu-Pu bonds in α-Pu. (b) Plot of the Debye-Waller factor versus temperature for the first and second shell U-U bonds in α-U as determined from fits to the Pu and U L_{III}-edge EXAFS data. The data are plotted along with fits generated using the correlated Debye model. For the α-U first shell, there is a sharp discontinuity in the slope of the Debye-Waller factor with temperature near the CDW transition temperature T_{CDW}. The correlated Debye model is only fit to points for temperatures $T > T_{CDW}$ for the α-U first shell.

reported to be half of this value.[12–15] It may be necessary to revisit the diffraction analyses and see which value is correct.

In order to explore what the EXAFS data can tell us about the CDW-modulated α-U phase, we apply two different models to the temperature-dependent EXAFS data series. In the first model, the low-temperature α-U series was fit again with the assumption that the Debye-Waller factor of the bonds is constant at the value determined from a fit to the $T=55$ K data ($\sigma^2_{1.55\ K}=0.00207$ Å^2) and the number of bonds at $R=2.73$ Å varies with temperature. For a normal Debye temperature dependence, the Debye-Waller factor should be nearly constant at these low temperatures. At and below $T=25$ K, the coordination number of 2.93 ± 0.05 is consistent with 3.0, the value expected for the square-wave CDW state. Above $T=25$ K, the coordination number drops linearly to 2.0 at $T=55$ K (which is its defined value at this temperature). For $T \geqslant 55$ K, it is assumed that the CDW structure no longer exists and the coordination number at $R=2.73$ Å remains at 2.0, the value for the unmodulated α-U structure. The low-temperature coordination number of 3.0 would correspond to a splitting of the 2.84 Å bonds along (100) equally into one bond at 2.73 Å and one at 2.95 Å in a square-wave modulation. Then the FT peak at $R=2.73$ Å is composed of the two 2.73 Å bonds in the $\langle 100 \rangle$ plane perpendicular to the (100) direction and one CDW-modulated bond along (100) at 2.84 Å $-2\varepsilon=2.73$ Å. A sine-wave modulation or phase-slipped sine-wave modulation in displacements would have contributions at a bond length ranging from 2.85 Å -2ε to 2.85 Å $+2\varepsilon$ which would result in less than one atom per unit cell contributing at $R=2.73$ Å on average in the (100) direction. This would result in a fit to the EXAFS data FT with less magnitude in the first peak, which is in disagreement with the data.

TABLE V. Correlated Debye temperatures θ_{cD} in Kelvin for the Pu-Pu and U-U bonds in α-Pu and α-U phases, respectively, as determined from the fit results in Tables III and IV. Results are presented for both the first and second nearest neighbor shells. The correlated Debye model was fit to the Debye-Waller factors for the α-U first shell only for temperatures above $T_{CDW} \approx 45$ K. The entire temperature range was used for the fit to the α-U second shell Debye-Waller factors, and for the fits to both α-Pu shell Debye-Waller factors.

Phase	First shell θ_{cD} (K)	Second shell θ_{cD} (K)
α-Pu	162 ± 5 K	147 ± 4 K
α-U	199 ± 3 K ($T \geqslant 55$ K only)	195 ± 3 K (entire T range)

In addition, the coordination number remains above 2.80 until above $T=25$ K, when it drops off quickly with temperature until it reaches the unmodulated value of 2.0 above $T_{CDW}=43$ K. The start of the sharper decrease in coordination number is at a temperature similar to the lock-in temperature of the CDW reciprocal lattice vector, $T_{lock\text{-}in}=22$ K.[13,14] These results suggest that the squaring of the displacement wave decreases with temperature for $T > T_{lock\text{-}in}$, and the CDW disappears above T_{CDW}.

Since the coordination numbers and Debye-Waller factors are highly correlated variables in any fit of EXAFS amplitudes, it is appropriate to look at the fitting of the CDW thermal behavior in another way by instead fixing the coordination number and varying the Debye-Waller factor. Another approach to quantifying the properties of the CDW

with the EXAFS data is to split the FT peak at 2.73 Å into two contributions—two unmodulated bonds in the ⟨100⟩ plane and one bond along (100) with its bond length modulated from 2.84 Å to 2.73 Å. The corresponding CDW-lengthened bond along (100) with $R=2.95$ Å is also included in the fit, and its Debye-Waller factor is set equal to that of the $R=2.73$ Å CDW bond. The Debye-Waller factors of the CDW bonds are set equal and allowed to vary. The Debye-Waller factor of the 2.73 Å non-CDW bonds in the ⟨100⟩ plane is set to the limiting value of the correlated Debye model fit at $T=0$ K($\sigma^2_{\text{stat}}=0.001\,82$ Å). This assumption is supported by the correlated Debye behavior and first shell correlated Debye temperature of $\theta_{cD}(\alpha\text{-U})=199\pm3$ K for the EXAFS above T_{CDW} seen in Fig. 9(b), for which the only bonds of length 2.73 Å are the bonds perpendicular to (100) in unmodulated α-U. With this model, the temperature dependence of the Debye-Waller factor of the CDW bonds along (100) is very steep. The correlated Debye model is fit to the temperature dependence of the CDW bond Debye-Waller factor, with a resulting correlated Debye temperature of 61 ± 5 K, much lower than the 199 ± 3 K measured for the 2.73 Å bonds at higher temperatures. The lower correlated Debye temperature should not be taken quantitatively but rather as an indicator of the softness of the bonds along the (100) due to the soft phonon. Since the force constant f_E of the bond vibration is related to the square of the correlated Debye temperature, $f_E \propto \theta^2_{cD}$, this suggests that the force constants of the CDW-modulated bonds are approximately an order of magnitude weaker than those of the nonmodulated bonds.

For temperatures $T=55$ K and above, where the structure should be unmodulated α-U, a peak at $R=2.84$ Å is expected. However, placing a component at this bond length significantly worsens the fits to the EXAFS data at these temperatures. This suggests that the amplitude of the $R=2.84$ Å bonds' contribution to the EXAFS is very low at and above $T=55$ K. Since the unmodulated α-U structure is known, the reduced amplitude must be due to a high Debye-Waller factor for the 2.84 Å bonds at these temperatures. Such a high Debye-Waller factor is unusual at these temperatures but may be possible due to the very soft phonon behavior along (100), which is the direction of the $R=2.84$ Å bond. Along with the CDW modeling of the EXAFS described above, this suggests that the CDW component of the EXAFS damps out very quickly with temperature. The rapid increase of the bond vibrational amplitude with temperature is related to the unusual softening of the $\mathbf{q}\approx(0.5,0,0)$ phonon frequency in α-U at lower temperatures, as well as the normal increase in vibration amplitude with temperature. Correlated "optical" motion also tends to increase the EXAFS Debye-Waller factor relative to the XRD or neutron diffraction Debye-Waller factor, since the EXAFS Debye-Waller factor measures the spread in the bond length distribution while the diffraction Debye-Waller factor measures the distribution in individual atom positions.

The temperature-dependent EXAFS data below T_{CDW} are consistent with a square-wave CDW along (100) whose contribution to the EXAFS is rapidly damped with a temperature due to the increase in optical vibrational motion along the (100) direction. The condensation of the soft optical phonon along (100) into the CDW for $T<T_{\text{CDW}}$ is consistent with these EXAFS results.

D. Coherence length of the CDW

Due to the anisotropic local bond length distribution in α-U, we have been able to observe the structure of the CDW in a polycrystalline α-U sample using temperature-dependent EXAFS. Previous structural observations of the CDW in α-U have used single-crystal specimens only.[2,7–14] Applying the Scherrer equation to the peak widths in the XRD profile of our α-U sample, the average crystallite grain size was found to be 70 ± 10 nm. This value sets an upper limit on the length scale required to stabilize the charge density wave within an α-U particle.

V. CONCLUSION

The EXAFS of the low-symmetry α-Pu and α-U phases were measured over a range of temperatures from $T=10$ K to room temperature. This study represents the first EXAFS measurement of the α-U phase, while the α-Pu EXAFS are a significant improvement in resolution compared to the previous EXAFS result.[29] In α-Pu, destructive and constructive EXAFS interferences, respectively, are observed between the subshells in the first and second nearest neighbor shells. In α-U, however, the expected destructive interference in the first shell between bonds at 2.73 Å and 2.84 Å is not observed, and at the lowest temperatures ($T\leqslant T_{\text{CDW}}\approx43$ K), the amplitude of the first shell EXAFS FT peak is increased above that expected for the unmodulated α-U structure. The amplitude of this FT peak decreases rapidly with temperature relative to the other FT peaks for $T<55$ K. In addition, at $T=55$ K and above, the expected unmodulated α-U bonds along (100) with length 2.84 Å do not contribute to the EXAFS. These anomalies between the measured and predicted EXAFS are explained by the existence of the CDW, as well as the softness of the phonon along the (100) direction.

The temperature dependence of the first-shell EXAFS Debye-Waller factor is fit well by a correlated Debye model over all temperatures for α-Pu, and for temperatures $T>T_{\text{CDW}}$ for α-U. The measured correlated Debye temperatures of $\theta_{cD}(\alpha\text{-Pu})=162\pm5$ K and $\theta_{cD}(\alpha\text{-U})=199\pm3$ K agree well with earlier values determined from heat capacity measurements. Below T_{CDW}, the Debye-Waller factor of the α-U first shell drops rapidly. In addition, different peaks in the α-U EXAFS FT behave very differently with temperature, indicating softer thermal behavior of bonds along the (100) direction. This behavior is attributed to the formation of the CDW along (100). Modeling the bond length distribution due to the CDW displacement wave suggests a partially squared CDW with a displacement wave amplitude of $\varepsilon=0.05\pm0.02$ Å. A pure sine wave CDW does not produce enough amplitude at the shortest bond length (2.73 Å) to satisfactorily reproduce the data at the lowest temperatures. The CDW bond contribution is seen to decay rapidly with

temperature, in agreement with the interpretation of the CDW as the condensation of the soft phonon mode. To our knowledge, our observation of the structure of the CDW in α-U is the first for a polycrystalline α-U sample, and sets a limit on the coherence length needed to stabilize the α-U CDW at 70 ± 10 nm, the grain size within our sample.

An important future experiment would be to add polarization dependence to the temperature-dependent α-U EXAFS, using the linear polarization of a synchrotron x-ray beam and either a single-crystal α-U sample or micro-EXAFS capability on a single α-U grain. Although the polarization dependence of the L_{III} absorption edge is less than that of the K edge, aligning the x-ray electric field parallel or perpendicular to the CDW (100) direction could enhance the contrast between CDW-related and non-CDW-related bonds and give improved structural information about the CDW. In addition, differences in the thermal behavior of the EXAFS between single-crystal and polycrystalline samples could be observed.

ACKNOWLEDGMENTS

The authors would like to thank Dr. Cheng Saw at LLNL for performing the XRD measurements on the samples. This work (UCRL-JRNL-206377) was performed under the auspices of the U.S. Department of Energy by University of California Lawrence Livermore National Laboratory under Contract No. W-7405-Eng-48, under LDRD funding. Portions of this research were carried out at the Stanford Synchrotron Radiation Laboratory, a national user facility operated by Stanford University on behalf of the U.S. Department of Energy, Office of Basic Energy Sciences. This work was partially supported (C.H.B.) by the Office of Basic Energy Sciences, Chemical Sciences Division of the U. S. DOE, Contract No. DE-AC03-76SF00098.

[1] W. H. Zachariasen and F. H. Ellinger, Acta Crystallogr. **16**, 777 (1963).
[2] C. S. Barrett, M. H. Mueller, and R. L. Hitterman, Phys. Rev. **129**, 625 (1963).
[3] P. Söderlind, O. Eriksson, B. Johansson, J. M. Willis, and A. M. Boring, Nature (London) **374**, 524 (1995).
[4] J. L. Smith and E. A. Kmetko, J. Less-Common Met. **90**, 83 (1983); S. S. Hecker, MRS Bull. **26**, 672 (2001).
[5] J. M. Willis and O. Eriksson, Phys. Rev. B **45**, 13879 (1992).
[6] L. F. Timofeeva, in *Aging Studies and Lifetime Extension of Materials*, edited by L. G. Mallinson (Kluwer Academic Plenum Publishers, New York 2001), p. 191.
[7] W. P. Crummett, H. G. Smith, R. M. Nicklow, and N. Wakabayashi, Phys. Rev. B **19**, 6028 (1979).
[8] H. G. Smith, N. Wakabayashi, W. P. Crummett, R. M. Nicklow, G. H. Lander, and E. S. Fisher, Phys. Rev. Lett. **44**, 1612 (1980).
[9] J. C. Marmeggi, A. Delapalme, G. H. Lander, C. Vettier, and N. Lehner, Solid State Commun. **43**, 577 (1982).
[10] J. C. Marmeggi, A. Delapalme, G. H. Lander, and C. Vettier, Physica B **120**, 263 (1983).
[11] H. G. Smith and G. H. Lander, Phys. Rev. B **30**, 5407 (1984).
[12] S. van Smaalen and T. F. George, Phys. Rev. B **35**, 7939 (1987).
[13] J. C. Marmeggi, G. H. Lander, S. van Smaalen, T. Brückel, and C. M. E. Zeyen, Phys. Rev. B **42**, 9365 (1990).
[14] G. Grübel, J. D. Axe, D. Gibbs, G. H. Lander, J. C. Marmeggi, and T. Brückel, Phys. Rev. B **43**, 8803 (1991).
[15] G. H. Lander, E. S. Fisher, and S. D. Bader, Adv. Phys. **43**, 1 (1994).
[16] M. E. Manley, B. Fultz, R. J. McQueeney, C. M. Brown, W. L. Hults, J. L. Smith, D. J. Thoma, R. Osborn, and J. L. Robertson, Phys. Rev. Lett. **86**, 3076 (2001).
[17] D. Koningsberger and R. Prins, in, *X-Ray Absorption: Principles, Applications, Techniques of EXAFS, SEXAFS, and XANES* (Wiley, New York, 1988).
[18] R. O. A. Hall and M. J. Mortimer, J. Low Temp. Phys. **27**, 313 (1977).
[19] J. Crangle and J. Temporal, J. Phys. F: Met. Phys. **3**, 1097 (1973).
[20] E. S. Fisher and D. Dever, Phys. Rev. **170**, 607 (1968).
[21] J. C. Lashley, B. E. Lang, J. Boerio-Goates, B. F. Woodfield, G. M. Schmiedeshoff, E. C. Gay, C. C. McPheeters, D. J. Thoma, W. L. Hults, J. C. Cooley, R. J. Hanrahan, Jr., and J. L. Smith, Phys. Rev. B **63**, 224510 (2001).
[22] M. E. Manley, B. Fultz, D. W. Brown, B. Clausen, A. C. Lawson, J. C. Cooley, W. L. Hults, R. J. Hanrahan, Jr., J. L. Smith, and D. J. Thoma, Phys. Rev. B **66**, 024117 (2002).
[23] L. E. Cox, R. Martinez, J. H. Nickel, S. D. Conradson, and P. G. Allen, Phys. Rev. B **51**, 751 (1995).
[24] P. Faure, B. Deslandes, D. Bazin, C. Tailland, R. Doukhan, J. M. Fournier, and A. Falanga, J. Alloys Compd. **244**, 131 (1996).
[25] N. Richard, P. Faure, P. Rofidal, J. L. Truffier, and D. Bazin, J. Alloys Compd. **271–273**, 879 (1998).
[26] P. G. Allen, A. L. Henderson, E. R. Sylwester, P. E. A. Turchi, T. H. Shen, G. F. Gallegos, and C. H. Booth, Phys. Rev. B **65**, 214107 (2002).
[27] M. Dormeval, N. Baclet, C. Valot, P. Rofidal, and J. M. Fournier, J. Alloys Compd. **350**, 86 (2003).
[28] J. Wong, M. Krisch, D. L. Farber, F. Occelli, A. J. Schwartz, T.-C. Chiang, M. Wall, C. Boro, and R. Xu, Science **301**, 1078 (2003).
[29] F. J. Espinosa, P. Villella, J. C. Lashley, S. D. Conradson, L. E. Cox, R. Martinez, B. Martinez, L. Morales, J. Terry, and R. A. Pereyra, Phys. Rev. B **63**, 174111 (2001).
[30] E. J. Nelson, K. J. M. Blobaum, M. A. Wall, P. G. Allen, A. J. Schwartz, and C. H. Booth, Phys. Rev. B **67**, 224206 (2003).
[31] T. M. Hayes and J. B. Boyce, in *Solid State Physics*, edited by H. Ehrenreich, F. Seitz, and D. Turnbull (Academic, New York, 1982), Vol. 37, p. 173.
[32] G. G. Li, F. Bridges, and C. H. Booth, Phys. Rev. B **52**, 6332 (1995).
[33] M. Newville, P. Livins, Y. Yacoby, J. J. Rehr, and E. A. Stern, Phys. Rev. B **47**, 14126 (1993).
[34] J. J. Rehr, J. Mustre de Leon, S. I. Zabinsky, and R. C. Albers,

Phys. Rev. B **44**, 4146 (1991).
[35] J. J. Rehr, J. Mustre de Leon, S. I. Zabinsky, and R. C. Albers, J. Am. Chem. Soc. **113**, 5135 (1991).
[36] E. D. Crozier, J. J. Rehr, and R. Ingalls, in *X-Ray Absorption: Principles, Applications, Techniques of EXAFS, SEXAFS, and XANES*, edited by D. Koningsberger and R. Prins (Wiley, New York, 1988), p. 373.
[37] G. B. Beni and P. M. Platzman, Phys. Rev. B **14**, 1514 (1976).
[38] A. C. Lawson, J. A. Goldstone, B. Cort, R. I. Sheldon, and E. M. Foltyn, J. Alloys Compd. **213/214**, 426 (1994).
[39] J. A. Lee and M. B. Waldron, in *Inorganic Chemistry*, Series 2 (University Park Press, Baltimore 1975), Vol. 7, Chap. 7, p. 250.
[40] J. C. Lashley, J. Singleton, A. Migliori, J. B. Betts, R. A. Fisher, J. L. Smith, and R. J. McQueeny, Phys. Rev. Lett. **91**, 205901 (2003).